Geosci. Model Dev. Discuss., 7, 3367–3402, 2014
www.geosci-model-dev-discuss.net/7/3367/2014/
doi:10.5194/gmdd-7-3367-2014

Geoscientific Model Development Discussions
Open Access

Sensitivity of aerosol extinction to new mixing rules in the AEROPT submodel of the ECHAM5/MESSy1.9 atmospheric chemistry (EMAC) model

K. Klingmüller[1], B. Steil[2], C. Brühl[2], H. Tost[3], and J. Lelieveld[1,2]

[1]The Cyprus Institute, P.O. Box 27456, 1645 Nicosia, Cyprus
[2]Max Planck Institute for Chemistry, P.O. Box 3060, 55020 Mainz, Germany
[3]Institut für Physik der Atmosphäre, Johannes Gutenberg-Universität Mainz, 55099 Mainz, Germany

Received: 18 February 2014 – Accepted: 23 April 2014 – Published: 16 May 2014

Correspondence to: K. Klingmüller (klingmueller@cyi.ac.cy)

Published by Copernicus Publications on behalf of the European Geosciences Union.

Abstract

The modelling of aerosol radiative forcing is a major cause of uncertainty in the assessment of global and regional atmospheric energy budgets and climate change. One reason is the strong dependence of the aerosol optical properties on the mixing state of aerosol components like black carbon and sulphates. Using a new column version of the aerosol optical properties and radiative transfer code of the atmospheric chemistry-climate model EMAC, we study the radiative transfer applying various mixing states. The aerosol optics code builds on the AEROPT submodel which assumes homogeneous internal mixing utilising the volume average refractive index mixing rule. We have extended the submodel to additionally account for external mixing, partial external mixing and multi-layered particles. Furthermore, we have implemented the volume average dielectric-constant and Maxwell Garnett Mixing rule. We performed regional case studies considering columns over China, India and Africa, corroborating much stronger absorption by internal than external mixtures. Well mixed aerosol is a good approximation for particles with a black carbon core, whereas particles with black carbon at the surface absorb significantly less. Based on a model simulation for the year 2005 we calculate that the global aerosol direct radiative-forcing for homogeneous internal mixing differs from that for external mixing by about 0.5 $W m^{-2}$.

1 Introduction

The limited quantitative understanding of aerosols chiefly contributes to uncertainty in radiative forcing estimates and climate simulations. The industrial era forcing (relative to the year 1750) by their direct radiative effect is estimated at $-0.27\ W m^{-2}$ with a 90 % uncertainty interval of $-0.77\ W m^{-2}$ to $0.23\ W m^{-2}$ (IPCC, 2013). The direct forcing is complemented by the indirect effects via cloud adjustment through the aerosol particles acting as cloud condensation nuclei, which is estimated at $-0.55\ W m^{-2}$ ($-1.33\ W m^{-2}$ to $-0.06\ W m^{-2}$) (IPCC, 2013). Despite the large uncertainty, the increase of the cloud

GMDD
7, 3367–3402, 2014

droplet number due to growing aerosol concentrations is generally recognized to exert a negative forcing and cooling effect by enhancing the reflection of solar radiation. While the indirect effects may have been large during the early period of industrialization and pollution emissions, their significance has probably been smaller in recent decades and will be in future (Carslaw et al., 2013). On the other hand, predominantly reflecting aerosol components are competing with absorbing carbonaceous components (black carbon) in the direct effect, and at present the uncertainty range does not rule out a net warming. Recently, the best estimate for the industrial era direct radiative forcing of atmospheric black carbon has been proposed to be as high as 0.71 $W m^{-2}$ (0.08 $W m^{-2}$ to 1.27 $W m^{-2}$) (Bond et al., 2013), which compensates to large extent the negative contributions of mineral dust, sulphate, nitrate and organic carbon. Thus, even to qualitatively capture the sign of the net direct effect, the uncertainties need to be drastically reduced in model simulations.

The large uncertainties have multiple origins, including insufficient knowledge of the emitted aerosol particles, strong spatial and temporal variations of the aerosol concentrations, and complex chemical ageing and coagulation processes transforming the aerosol particles during their lifetime in the atmosphere. A major source of uncertainty is the strong dependence of the aerosol optical properties on the mixing state of the aerosol components. This demands a better understanding of the mixing state found in atmospheric aerosols on the one hand, and on the other hand the implementation of realistic mixing states in climate models, in particular in global chemistry-climate models like the ECHAM/MESSy Atmospheric Chemistry model (EMAC) (Jöckel et al., 2005, 2006).

Most climate models assume the atmospheric aerosol mixture of chemical constituents to be either internal, assuming homogeneous particles, or external (Fig. 1). Generally, external mixtures are less absorbing than internal mixtures, as the increased cross section affected by absorbing components in an internal mixture outweighs the decreased absorption efficiency. Therefore, external and internal mixtures typically under- and overestimate, respectively, absorption of solar radiation, if not used

GMDD
7, 3367–3402, 2014

appropriately. Only few global simulations consider core-shell particles, e.g., Jacobson (2000, 2001); Kim et al. (2008).

Here we use the EMAC model, which includes the aerosol optical-properties submodel AEROPT (Lauer et al., 2007; Pozzer et al., 2012), which primarily mixes different aerosol components internally, assuming a homogeneous mixture. This rather idealised mixing state is probably representative of chemically aged particles and used for simplicity, but, as mentioned above, can overestimate aerosol absorption. Aerosol particles in reality form coated spheres or are externally mixed, especially close to the emission sources. Ideally, the model provides all mixing states from external mixing through core-shell mixing to well-mixed internal mixtures and calculates the optimal configuration online depending on chemical processing and coagulation during atmospheric transport. For this study, we have extended AEROPT by external mixing, partial external mixing, multi-layered particles and two alternative mixing rules. At this stage, the mixing state within each mode is chosen offline ahead of each simulation, whereas interactive computations are planned for future applications. However, as fresh black carbon is emitted into hydrophobic modes where it is separated from components in the hydrophilic modes to which it can subsequently be transferred, a transition from external to internal mixing is already accounted for, similarly as in Ghan et al. (2012).

A key aspect of this work is the comparison of internal and external mixing which we study in regional case studies and a global simulation. It provides an envelope of optical properties and their impact on the associated climate forcing by anthropogenic aerosol constituents for several mixing states. In addition, we address alternative mixing rules and core-shell particles for which we present regional results.

This article is structured as follows: we briefly review the relevant mixing states in Sect. 2, including the equations used in our aerosol optical-property code AEROPT. Section 3 describes how the aerosol optical-properties are processed in EMAC and introduces a column version of the submodels involved. Model results are presented in Sect. 4, including column results for test cases and regional case studies in Sect. 4.1 and global results in Sect. 4.2. We conclude with Sect. 5.

GMDD
7, 3367–3402, 2014

2 Aerosol mixing-states

In the presence of multiple aerosol components it becomes challenging to compute the optical parameters of the aerosol. The main characteristics of the scattering and absorption process can be simulated using three parameters, the extinction coefficient σ which is directly linked to the aerosol optical-thickness τ, the single-scattering albedo ω and the asymmetry factor γ,

$$\tau = \int \sigma \, \mathrm{d}z$$

$$\omega = \frac{\sigma_\mathrm{s}}{\sigma}$$

$$\gamma = \frac{1}{2} \int_{-1}^{1} \mu \, P(\mu) \, \mathrm{d}\mu, \tag{1}$$

where z denotes the vertical coordinate, σ_s the scattering part of the extinction coefficient, μ the cosine of the scattering angle and P the phase function. Assuming spherical particles, if there is only one component, these parameters can be computed straightforwardly using Mie theory and the corresponding refractive index of the component. However, if more than one component is involved, certain assumptions about the mixing state have to be made. The mixing states can be classified as either external (Fig. 1a) or internal (Fig. 1b and c).

2.1 External mixing

In an external mixture, each aerosol particle consists of only one component, however, different particles may consist of different components (Fig. 1a). In this case, the extinction coefficients of all components add up to the total extinction

$$\sigma = \sum_i \sigma_i, \tag{2}$$

GMDD
7, 3367–3402, 2014

where the index i identifies the component. The same applies to the scattering coefficient σ_s. The ratio of the scattering coefficient and the total extinction coefficient yields the single-scattering albedo,

$$\omega = \frac{\sigma_s}{\sigma} = \frac{\sum_i \sigma_{s,i}}{\sum_i \sigma_i} = \frac{\sum_i \sigma_i \ \omega_i}{\sum_i \sigma_i}. \quad (3)$$

The flux scattered with angle $\arccos(\mu)$ by component i is proportional to $P_i(\mu)\ \sigma_{s,i}$, so that the corresponding flux scattered by all components is proportional to

$$\sum_i P_i(\mu)\ \sigma_{s,i} = P(\mu)\ \sigma_s,$$

where P is the combined phase function of which the first moment, according to Eq. (1), yields the asymmetry factor of the mixture,

$$\gamma = \frac{1}{2} \int_{-1}^{1} \mu \ \frac{\sum_i P_i(\mu)\ \sigma_{s,i}}{\sigma_s} \ \mathrm{d}\mu = \frac{\sum_i \sigma_i \ \omega_i \ \gamma_i}{\sum_i \sigma_i \ \omega_i}. \quad (4)$$

Once the three parameters σ, ω and γ have been calculated according to Eqs. (2)–(4), the radiative transfer equation can be solved as for an aerosol with only one component.

2.2 Internal mixing

Internal mixing assumes that single aerosol particles themselves consist of different components (Fig. 1b and c). The simplest variant of internal mixing is based on the assumption that the different components are well mixed and form a homogeneous mixture inside the particles (Fig. 1c). In this case, the problem boils down to computing the refractive index of the mixture. Homogeneous internal mixing is a very common assumption and various mixing rules to compute the refractive index have been defined.

GMDD
7, 3367–3402, 2014

2.2.1 Mixing rules

The mixing rules utilised in this work are:

1. *Volume average refractive index mixing rule*: the complex refractive index m of the mixture is computed as an average of the indices m_i of the components, weighted with their volume fraction v_i,

$$m = \sum_i v_i m_i. \tag{5}$$

2. *Volume average dielectric constant mixing rule*: the complex dielectric constant $\varepsilon = m^2$ of the mixture is computed as an average of the constants ε_i of the components, weighted with their volume fraction v_i,

$$\varepsilon = \sum_i v_i \varepsilon_i. \tag{6}$$

3. *Maxwell Garnett mixing rule* (Garnett, 1904): the ansatz for the equation for the complex dielectric constant considers tiny inclusions embedded within a matrix of component M. Averaging the electric field over many inclusions yields the effective dielectric constant

$$\varepsilon = \varepsilon_{\mathrm{M}} \left(1 + \frac{3 \sum_i v_i \frac{\varepsilon_i - \varepsilon_{\mathrm{M}}}{\varepsilon_i + 2\varepsilon_{\mathrm{M}}}}{1 - \sum_i v_i \frac{\varepsilon_i - \varepsilon_{\mathrm{M}}}{\varepsilon_i + 2\varepsilon_{\mathrm{M}}}} \right). \tag{7}$$

   Note that despite of the spatial inhomogeneous ansatz, using this limit also implies homogeneously mixed aerosol particles.

The refractive index resulting from these mixing rules can be used as input for a Mie computation to obtain the extinction coefficient σ, single-scattering albedo ω and asymmetry factor γ.

GMDD
7, 3367–3402, 2014

A mixture of strongly and weakly absorbing components generally absorbs stronger if it is well mixed internally than if it is externally mixed, as the larger cross section affected by the strong absorber in an internal mixture overcompensates the effect of a reduced imaginary part of the refractive index.

2.2.2 Core-shell particles

Both, the external and homogeneous internal mixture are highly idealised models of the atmospheric aerosol. In reality, we can assume that often different aerosol components will neither coexist unaffected by each other, nor will they accumulate to homogeneous particles, but more likely form coated particles. Extensions of the Mie calculation to coated spheres and multilayered spheres, respectively, are presented in Toon and Ackerman (1981); Bohren and Huffman (2007) and Yang (2003).

The shell layers (including the core) themselves may consist of different, well mixed components. In that case, a mixing rule is used to compute the complex refractive index of each layer which then serves as input for the core-shell calculation.

In many cases, the calculations of aerosol optical properties for core-shell particles are limited by the results for external and homogeneous internal mixing (Jacobson, 2000). Core-shell particles with a strongly absorbing core coated by a weak absorber generally absorb more sunlight than an external mixture of the same components. This is due to lensing by the shell which effectively increases the cross section of the core. The lensing effect can result in absorption that is even stronger than of a well mixed internal mixture of the same components, depending on the Mie size-parameter under consideration.

3 Aerosol optical properties in EMAC

The model setup used in this work involves three submodels in the computation of the aerosol radiative-effect: GMXe, AEROPT and RAD4ALL. The aerosol model GMXe

GMDD
7, 3367–3402, 2014

(Pringle et al., 2010a, b) provides aerosol concentrations serving as input for AEROPT (Lauer et al., 2007; Pozzer et al., 2012), which computes the aerosol optical-properties. These are then accounted for by RAD4ALL (Jöckel et al., 2006) when solving the radiative-transfer equation and computing heating rates.

AEROPT computes for each cell of the grid representing the atmosphere and every RAD4ALL wavelength-band the aerosol optical-thickness τ, the single-scattering albedo ω and the asymmetry factor γ. To do so, AEROPT combines data for six aerosol modes, the Aitken, accumulation and coarse mode, all of which are treated separately for hydrophilic and hydrophobic components. The nucleation mode additionally accounted for by GMXe is neglected in AEROPT due to its insignificant impact on the radiative transfer. Besides combining the modes, AEROPT integrates the different components in each mode as well as four sub-bands per RAD4ALL shortwave band (cf. Fig. S1 in the Supplement).

Aerosols from different modes are considered externally mixed which is justified by the relatively small overlap of the mode size distributions. In contrast, within each mode the aerosol components in the standard AEROPT version are assumed to be internally mixed and the volume average refractive index mixing rule Eq. (5) is used.

In this work we use a modified version of AEROPT in which we have additionally implemented the volume average dielectric constant mixing rule Eq. (6) and the Maxwell Garnett mixing rule Eq. (7). Our code provides the option to use external mixing also within each mode. Moreover, we have substituted the Mie code used by standard AEROPT, BHMIE (Bohren and Huffman, 2007) as implemented in the libRadtran package (Mayer and Kylling, 2005), with SCATTNLAY (Peña and Pal, 2009), which computes the scattering functions also for coated spheres with multiple layers of coating according to Yang (2003). SCATTNLAY allows the use of a large number of shells so that it essentially covers the most general case of spherical symmetric particles. Configured to perform standard AEROPT mixing, our mixing algorithm is equivalent to that of AEROPT in MESSy version 2.42.

GMDD
7, 3367–3402, 2014

To perform regional sensitivity studies and to easily test new mixing states and other developments in the EMAC aerosol and radiation code, we have implemented a column model which calls the original EMAC subroutines to compute aerosol optical properties, radiative fluxes and heating rates for a vertical column of the atmosphere. The computational resources required for the column model are modest so that it can run on a common PC. Once implemented and tested in the column model, new features are immediately available for global model simulations.

4 Model results

4.1 Column model

4.1.1 Test cases

To evaluate the functionality of the extended AEROPT code and to obtain qualitative understanding of the optical properties of core-shell particles we use the column model to consider two test cases.

Large differences in aerosol absorption for internal and external mixtures, respectively, have been reported (Bohren and Huffman, 2007; Jacobson, 2000). Bohren and Huffman (2007) use an analytic approximation to illustrate that an internal mixture of a "black" and a "white" component can absorb more than twice as efficiently as an external mixture. As a benchmark for our extended AEROPT code, we provide the column model with the input used by Bohren and Huffman: for the black component the refractive index $m = 1.7 + i\ 0.7$ is used, for the white component $m = 1.55 + i10^{-6}$. The volume mixing ratio of the black component is assumed to be 1 %. The particle radius is varied, however in case of the external mixture the black particle radius is fixed at 0.05 µm.

Figure 2 shows the consistency of the single scattering albedo computed with AEROPT and the results of Bohren and Huffman (2007). Over the full range of radii,

GMDD
7, 3367–3402, 2014

well mixed particles absorb much more efficiently than externally mixed particles. Only for very small particles this efficiency is exceeded by core-shell particles, which for intermediate radii yield results between the well and externally mixed results. With increasing radius, the single scattering albedo of the external mixture is increasingly dominated by the black particles because, due to their constant radius, their total cross section remains constant whereas it decreases for the white particles. As a result, the single scattering albedo becomes smaller than that of core-shell particles, which would not be the case if equal radii for black and white particles had been assumed.

Figure 2 includes results obtained considering particles with sizes distributed according to a log-normal distribution with geometric standard deviation $\sigma_g = 1.59$, using the average mass particle radius for the abscissa and accordingly an average mass particle radius of 0.05 µm for black particles in the external mixture. Employing modes instead of single size particles has the side effect of smoothing the small scale variations of the result. As in the full EMAC computation, in the following test case, we exclusively consider log-normal modes.

For large particles (Mie size parameter $x \gg 1$) core-shell particles typically absorb less efficiently than internally mixed particles (though more efficiently than externally mixed particles of the same size). However, in the Mie regime ($x \approx 1$) this is not true in general, as can be seen from the leftmost part of Fig. 2 and more clearly in the test case shown in Fig. 3 (see also Fuller et al., 1999). The single scattering albedo is shown for a mixture of two components, one with refractive index $m = 1.75 + i\ 0.43$ ("black") resembling black carbon and the second with refractive index $m = 1.5 + i\ 0.02$ ("white") resembling a mixture of various scattering components typically found in the atmosphere. The black component is assumed to account for 2 % of the aerosol particle volume, the particle size is distributed according to a log-normal distribution with geometric standard deviation $\sigma_g = 1.59$ and the same median radius is used for all mixing states. For size parameters $x \lesssim 5$ the result for core-shell particles with a black core is very similar to that for well mixed particles with a slightly smaller single scattering albedo for size parameters $x \lesssim 2$. Since atmospheric aerosol size parameters

GMDD
7, 3367–3402, 2014

both above and below the intersection are relevant, only a full evaluation of all aerosol modes and wavelength bands can reveal which mixing state absorbs more efficiently. Less ambiguous is the comparison of well mixed to black coated spheres: in this example, even for small size parameters, the single scattering albedo of black coated particles is larger. A comparison of black-core and black-shell particles can also be found in Hong et al. (2008) from whom selected results have been re-evaluated with our code yielding good agreement.

Also apparent from Fig. 3 is the strong dependence of the single scattering albedo on the aerosol mode median Mie size parameter. Left and right of the curves' maximum, changes in the Mie size parameter, e.g., due to water uptake, can alter the scattering albedo more drastically than changing the mixing state.

Figures 4 and 5 show that qualitatively the result in Fig. 3 also applies if the mixing ratio and standard deviation are varied. The relative difference of absorption efficiency for well mixed and core-shell particles, $(\omega_{\text{well mixed}} - \omega_{\text{core shell}})/(1 - \omega_{\text{well mixed}})$, is shown for black-core particles (Fig. 4) and black-coated particles (Fig. 5). Only the location of the intersection in the former case and the value of the difference plotted in both cases varies. For a fixed geometric standard deviation of $\sigma_g = 1.59$ (left panels), depending on the Mie size parameter and the black volume fraction, black-core particles can absorb 16 % less or 8 % more efficiently than well-mixed particles. Black coated particles, the absorption of which in this example never exceeds that of well-mixed particles, can absorb up to almost 20 % less efficiently than the homogeneously mixed particles.

The refractive index $m = 1.75 + i\ 0.43$ of the black component corresponds to the black carbon value (at 600 nm wavelength) in the OPAC 3.1 database (Hess et al., 1998) which is used by EMAC. In the literature, larger values for both, real and imaginary part, have been suggested (Bond and Bergstrom, 2006). As Fig. 6 shows, the above results change mostly quantitatively when changing the refractive indices. However, increasing the imaginary part of the refractive index for the black particles reduces the Mie size parameter range where core-shell particles absorb more efficiently than well mixed particles. Consequently, in a full radiative transfer computation considering

GMDD
7, 3367–3402, 2014

many different Mie size parameters it cancels to a lesser extent the effect of the remaining parameter range, decreasing the absorption efficiency of core-shell particles relative to that of well mixed particles.

Different mixing ratios, refractive indices, median Mie size parameters, mode widths and wavelengths are relevant to the single scattering albedo in the atmosphere. Consequently, more elaborate case studies are required to extent our reasoning to atmospheric aerosols, which will be addressed in the following section.

4.1.2 Regional sensitivity studies

To study regional mixing-state sensitivity under realistic conditions, we employ the column model and introduce aerosol concentrations from a global simulation for the year 2005 using the same model setup as Pozzer et al. (2012), which is also used in Sect. 4.2. For each region, we consider days on which the corresponding column is cloud free at noon local time. The concentrations and additional data required for the flux and heating rate computation is taken from the model time step with the smallest zenith angle. The radiative flux is evaluated every 18 min so that all case studies are performed within nine minutes of solar noon. The geometric standard deviation of the hydrophilic and hydrophobic coarse mode is $\sigma_g = 2.2$ and $\sigma_g = 2$, respectively, and $\sigma_g = 1.59$ for all other modes.

The refractive indices are taken from the OPAC 3.1 database (Hess et al., 1998) (black carbon, mineral dust) and the HITRAN 2004 database (Rothman et al., 2005) (organic carbon, sea salt, ammonium sulphate, water). The mineral dust and organic carbon values have been complemented by data from I. N. Sokolik (unpublished data, 2005) and Kirchstetter et al. (2004), respectively. The data for ammonium sulphate also serves as default for other components. The indices are plotted in Fig. S1 in the Supplement.

GMDD
7, 3367–3402, 2014

Northern China

The high aerosol concentrations and abundance of aerosol components make the coastal areas in northern China particularly interesting for studying mixing state sensitivity. One may assume that especially close to the source regions aerosols are not homogeneously mixed. We focus on a model column centred at 38.7° N, 117.0° E adjacent to Bohai Bay southeast of Beijing in October. For the given model resolution this column covers the area between 38.1° N, 116.4° E and 39.3° N, 117.6° E (see inset in Fig. 7). The vertical profiles of the concentrations in each mode are shown in Fig. 7. In particular in the accumulation mode, which is the most relevant for solar radiation scattering, the concentrations are high and various components are accompanied by a small but significant fraction of black carbon.

The resulting optical properties, radiative flux and temperature tendency are shown in Fig. 8. In the leftmost panel, the aerosol optical depth (AOD) τ is shown for internal mixing using the average refractive index, external mixing and an intermediate mixing state in which only black carbon is externally mixed with an internal mixture of the remaining components. Also shown are the results for particles with a black carbon core and shell, respectively, where the rest of the components are well mixed using the average refractive index. The sensitivity to the mixing state appears to be small.

The RAD4ALL shortwave-band covering the lower end of the solar wavelength spectrum (0.25–0.69 µm) dominates not only because it accounts for almost 50 % of the incoming energy but also the corresponding aerosol optical depth is largest. For clarity, the single scattering albedo in the second panel is shown for this band only. In contrast to the optical depth, the single scattering albedo of the internal mixture differs significantly from that of the external mixture. This is primarily related to the black carbon component as can be seen from the intermediate mixing state (dashed line): even though only black carbon is externally mixed, we compute an effect comparable to that for the external mixture. This is even more remarkable considering the fact that the volume of the black carbon particles accounts for only a small fraction of the total

GMDD
7, 3367–3402, 2014

particle volume as illustrated in Fig. 7. Assuming that black carbon forms the core of the aerosol particles yields a single scattering albedo only marginally larger than the result for well mixed particles. In contrast, assuming black carbon to coat the rest of the components results in significantly less absorption.

The difference between single scattering albedo for internal and external mixing is much more evident than that between the different variants of homogeneous internal mixing in the centre panel, namely the average refractive index mixing rule, the average dielectric constant mixing rule and the Maxwell Garnett mixing rule. For the latter we consider water as matrix (black and organic carbon in the insoluble Aitken mode are well mixed using the average refractive index, in the other two dry, insoluble modes there is only one component). It yields slightly less absorption than the average refractive index mixing rule. In contrast, the average dielectric constant mixing rule yields stronger absorption and deviates more strongly from the result obtained using the average refractive index mixing rule. The difference is comparable to that for black carbon coated particles, but has the opposite sign. We conclude that it is most relevant to correctly apply internal or external mixing. The results are less, but still significantly sensitive to the choice of the internal mixing state (well mixed or core shell) and the mixing rule, which are both about equally relevant.

The lower single scattering albedo of the internal mixtures is reflected by the radiative flux profile in the fourth panel. The stronger absorption in the atmosphere leads to a larger net downward shortwave flux at the top of the atmosphere whereas this flux is reduced at the bottom of the atmosphere. In this example, switching from external to internal mixing alters the flux by 13 $\mathrm{W\,m^{-2}}$ at the top of the atmosphere and $-20\ \mathrm{W\,m^{-2}}$ at the surface, whereas the longwave flux is essentially unaffected. As a consequence, for internal mixing additionally 33 $\mathrm{W\,m^{-2}}$ are absorbed within the troposphere. This increases the heating rate within the troposphere as shown in the rightmost panel. Here, internal mixing yields an additional contribution to the heating of the troposphere at noon of up to 2.9 $\mathrm{K\,day^{-1}}$.

GMDD
7, 3367–3402, 2014

The two main effects of increasing aerosol absorption are shown by the right two profiles. Firstly, the stronger heating of the troposphere impacts the regional dynamics of the atmosphere. Secondly, the increased downward flux at the top of the atmosphere increases the warming. We will quantify this effect on larger scales in section Sect. 4.2.

Sahara

The exceptionally high aerosol concentrations found over northern Africa are dominated by Saharan mineral dust. Consequently, despite a strong aerosol radiative effect, we expect a small mixing state sensitivity. Figure 9 shows the aerosol concentrations in a column over the Niger–Chad border (centred at 19.63° N, 15.75° E, see inset in Fig. 9) by the end of June. By far the highest concentration is found in the hydrophobic coarse mode, exclusively represented by mineral dust.

This dominance of large aerosol particles is reflected by an almost negligibly small wavelength dependence of the aerosol optical depth shown in Fig. 10 and correspondingly a small Ångström exponent. Thus, larger wavelengths are more strongly affected by extinction than in the previous example and therefore the single scattering albedo is shown for all shortwave bands. Like the optical depth, the single scattering albedo shows very little sensitivity to the mixing state. The minor sensitivity which mostly occurs at high altitudes where the dust concentration vanishes does not appear in the flux profile and the heating rate.

Sichuan Basin, Gangetic Plain, eastern Niger Delta

Figure 11 combines results for three regions with high sensitivity to the aerosol mixing-state: over the Sichuan Basin in southwestern China aerosol compositions are similar to that over the coastal areas in northern China but with even higher concentrations, the Gangetic Plain shows a larger fraction of organic carbon, and in the eastern Niger Delta black and organic carbon are combined with large amounts of mineral dust.

GMDD
7, 3367–3402, 2014

As in the northern China example, the single scattering albedo for particles with a black carbon core is very close to that for homogeneously internally mixed particles. It can be both slightly smaller and larger, similar to the result in Fig. 3. In contrast, absorption by particles coated with black carbon is always smaller than by well mixed particles. The single scattering albedo over the eastern Niger Delta, for example, shows that the difference can be almost half as large as that between the result for externally mixed black carbon and well mixed particles. While spherical symmetric coating of particles by black carbon is unlikely to be found in reality, black carbon inclusions at the edge of aerosol particles have been observed (Adachi et al., 2010) and made responsible for reduced absorption enhancement in internal mixtures (Cappa et al., 2012). Typically, the specific absorption tends to decrease if the black carbon is further away from the particle centre and closer to the surface (Fuller et al., 1999). Small differences between the radiative forcing of well mixed and black carbon core particles have been reported previously (Kim et al., 2008) and larger differences as found in Jacobson (2001) might be attributed to a different black carbon refractive index and particle size distribution.

Generally, the sensitivity of the shortwave flux at the surface is higher than at the TOA. This difference increases with decreasing single scattering albedo. The more strongly absorbing the aerosol, the less scattered radiation reaches the TOA, decreasing the sensitivity of the TOA flux. In addition, the sensitivity at the surface is higher with a larger total amount of absorbed radiation, i.e., a smaller single scattering albedo. Over the eastern Niger Delta, with a relatively low single scattering albedo of about 0.7, the surface flux for internal and external mixing, respectively, differs by $-25\,\mathrm{W\,m^{-2}}$ which is twice as large as the difference at the TOA ($12\,\mathrm{W\,m^{-2}}$).

4.2 Global sensitivity

To estimate the mixing state sensitivity of the global radiative forcing by aerosols, we simulate the year 2005 using the model version employed in Pozzer et al. (2012), where the setup is described extensively. In EMAC the version MESSy 1.9 is utilised

GMDD
7, 3367–3402, 2014

in combination with ECHAM 5.3.01 using the horizontal resolution T106 ($\approx 1.1^\circ \times 1.1^\circ$) and 31 vertical layers up to 10 hPa in the lower stratosphere. The model dynamics are nudged to meteorological analyses of the European Centre for Medium-range Weather Forecasts (ECMWF) and the prognostic radiative-transfer calculation uses the Tanre aerosol climatology (Tanre et al., 1984).

In each model time step we call our modified AEROPT routine multiple times to compute the aerosol optical properties for different mixing states. Accordingly, we use multiple diagnostic calls to the radiation submodel RAD4ALL to evaluate the corresponding fluxes and heating rates, thereby obtaining instantaneous radiative forcings not including dynamical feedbacks.

Figure 12 compares the annual average of the shortwave fluxes for internal (int) and external (ext) mixing as well as the intermediate mixing state from Sect. 4.1.2 in which only black carbon is externally mixed (bcext).

The top of the atmosphere (TOA) forcing is affected by the mixing state most significantly over China and the Ganges-Brahmaputra-Meghna basin. Over China, the annual average of the difference between the TOA flux for internal and external mixing $F_{\mathrm{int}} - F_{\mathrm{ext}}$ reaches values in excess of $8\,\mathrm{W\,m^{-2}}$. While the sensitivity is largely correlated to the AOD as published in Pozzer et al. (2012), there are noticeable exceptions. Most strikingly, northern Africa shows very little sensitivity, whereas the AOD in that region is among the highest worldwide. As demonstrated with the Saharan column in Sect. 4.1.2, the reason is that the AOD in northern Africa is dominated by mineral dust, while other aerosol components including black carbon and thus aerosol mixing play a minor role. The same applies to the Taklamakan Desert in northwest China. In Central Africa, on the other hand, biomass burning aerosols are important and again the contribution by black carbon gives rise to a significant effect by the mixing state.

The change in TOA flux goes hand in hand with an – even slightly larger – difference in the surface flux with opposite sign. As the difference in flux absorbed by the atmosphere thus regionally exceeds $18\,\mathrm{W\,m^{-2}}$ on the annual average, we expect

GMDD
7, 3367–3402, 2014

the regional atmospheric dynamics to be sensitive to alterations of the aerosol mixing scheme.

As in the regional case studies described in Sect. 4.1.2, also globally the mixing state sensitivity is mostly related to black carbon. The difference between the TOA flux for internal mixing and the intermediate mixing state $F_{\text{int}} - F_{\text{bcext}}$ shows to a large extent the same pattern as that between the flux for internal and external mixing. Even though the difference is smaller, black carbon generally accounts for more than half of the total effect, with the difference reaching 7 W m^{-2} over China. This is consistent with our results for the regional single scattering albedos in Figs. 8 and 11.

The global average of the TOA shortwave flux difference amounts to 0.53 W m^{-2} when comparing the internal mixture to the fully external mixture and 0.35 W m^{-2} when comparing to the intermediate mixing state. Being of the same order of magnitude as current estimates for the aerosol direct radiative forcing, these values suggest a considerable mixing state sensitivity of the global energy budget, in particular because it may be assumed that black carbon is predominantly of anthropogenic origin. This supports results of prior studies: the global average of 0.35 W m^{-2} is between that in Chung and Seinfeld (2005), where the difference of the forcing for the well mixed internal mixture and the forcing for externally mixed elemental carbon is estimated at 0.27 W m^{-2} and Jacobson (2000), estimating this to be 0.51 W m^{-2}.

5 Conclusions

We have implemented revised aerosol mixing states in the EMAC submodel AEROPT to study the sensitivity for various types of particle components worldwide.

The regional case studies performed with a new column version of the EMAC radiation code as well as our global results reveal a significant sensitivity to a transition from external to internal mixing, which increases aerosol absorption by black carbon. The difference depends on the local concentrations of the aerosol components which cannot be taken into account using a constant enhancement factor applied to the external

GMDD
7, 3367–3402, 2014

mixing result. Our implementations of internal and external mixing yield results consistent with calculations by Bohren and Huffman (2007), and the strong sensitivity of the global radiative forcing to excluding black carbon from the otherwise internal aerosol mixture supports the findings by Jacobson (2000) and Chung and Seinfeld (2005).

In EMAC, the AEROPT submodel combines internal mixing within and external mixing between the modes calculated with the GMXe submodel, and by allowing aerosol particles to switch between modes the model captures the effect of changing optical properties through chemical ageing and coagulation. Our results underscore the importance of modelling these processes with the appropriate level of detail to adequately account for the aerosol radiative forcings and climate effects.

In our regional case studies, homogeneous internal mixing provides a good approximation for the optical properties of particles with a strongly absorbing core. However, it overestimates absorption by particles with strongly absorbing coating. Therefore, we conclude that it is generally recommended to take the inner structure of internally mixed particles into account.

Code availability

The Modular Earth Submodel System (MESSy) is continuously further developed and applied by a consortium of institutions. The usage of MESSy and access to the source code is licenced to all affiliates of institutions which are members of the MESSy Consortium. Institutions can be a member of the MESSy Consortium by signing the MESSy Memorandum of Understanding. More information can be found on the MESSy Consortium Website (http://www.messy-interface.org). The submodel AEROPT is part of MESSy. Regarding the column model and mixing rules used in this study but not yet included in released MESSy versions, the author Klaus Klingmüller (klingmueller@cyi.ac.cy) can be contacted directly.

GMDD
7, 3367–3402, 2014

The Supplement related to this article is available online at doi:10.5194/gmdd-7-3367-2014-supplement.

Acknowledgements. We thank Andrea Pozzer for providing the EMAC setup used in Sect. 4.2. The research leading to these results has received funding from the European Research Council under the European Union's Seventh Framework Programme (FP7/2007-2013)/ERC grant agreements no 226144 and no 261600.

References

Adachi, K., Chung, S. H., and Buseck, P. R.: Shapes of soot aerosol particles and implications for their effects on climate, J. Geophys. Res.-Atmos., 115, D15206, doi:10.1029/2009JD012868, 2010. 3383

Bohren, C. F. and Huffman, D. R.: Absorption and Scattering of Light by Small Particles, Wiley-VCH Verlag GmbH, 2007. 3374, 3375, 3376, 3386, 3392

Bond, T. C. and Bergstrom, R. W.: Light absorption by carbonaceous particles: an investigative review, Aerosol Sci. Tech., 40, 27–67, doi:10.1080/02786820500421521, 2006. 3378

Bond, T. C., Doherty, S. J., Fahey, D. W., Forster, P. M., Berntsen, T., Deangelo, B. J., Flanner, M. G., Ghan, S., Kärcher, B., Koch, D., Kinne, S., Kondo, Y., Quinn, P. K., Sarofim, M. C., Schultz, M. G., Schulz, M., Venkataraman, C., Zhang, H., Zhang, S., Bellouin, N., Guttikunda, S. K., Hopke, P. K., Jacobson, M. Z., Kaiser, J. W., Klimont, Z., Lohmann, U., Schwarz, J. P., Shindell, D., Storelvmo, T., Warren, S. G., and Zender, C. S.: Bounding the role of black carbon in the climate system: a scientific assessment, J. Geophys. Res.-Atmos., 118, 5380, doi:10.1002/jgrd.50171, 2013. 3369

Cappa, C. D., Onasch, T. B., Massoli, P., Worsnop, D. R., Bates, T. S., Cross, E. S., Davidovits, P., Hakala, J., Hayden, K. L., Jobson, B. T., Kolesar, K. R., Lack, D. A., Lerner, B. M., Li, S.-M., Mellon, D., Nuaaman, I., Olfert, J. S., Petäjä, T., Quinn, P. K., Song, C., Subramanian, R., Williams, E. J., and Zaveri, R. A.: Radiative absorption enhancements due to the mixing state of atmospheric black carbon, Science, 337, 1078–1081, doi:10.1126/science.1223447, 2012. 3383

Carslaw, K. S., Lee, L. A., Reddington, C. L., Pringle, K. J., Rap, A., Forster, P. M., Mann, G. W., Spracklen, D. V., Woodhouse, M. T., Regayre, L. A., and Pierce, J. R.:

GMDD
7, 3367–3402, 2014

Large contribution of natural aerosols to uncertainty in indirect forcing, Nature, 503, 67–71, doi:10.1038/nature12674, 2013. 3369

Chung, S. H. and Seinfeld, J. H.: Climate response of direct radiative forcing of anthropogenic black carbon, J. Geophys. Res.-Atmos., 110, D11102, doi:10.1029/2004JD005441, 2005. 3385, 3386

Fuller, K. A., Malm, W. C., and Kreidenweis, S. M.: Effects of mixing on extinction by carbonaceous particles, J. Geophys. Res.-Atmos., 104, 15941, doi:10.1029/1998JD100069, 1999. 3377, 3383

Garnett, J. C. M.: Colours in metal glasses and in metallic films, Philos. T. R. Soc. Lond., 203, 385–420, doi:10.1098/rsta.1904.0024, 1904. 3373

Ghan, S. J., Liu, X., Easter, R. C., Zaveri, R., Rasch, P. J., Yoon, J.-H., and Eaton, B.: Toward a minimal representation of aerosols in climate models: comparative decomposition of aerosol direct, semidirect, and indirect radiative forcing, J. Climate, 25, 6461–6476, doi:10.1175/JCLI-D-11-00650.1, 2012. 3370

Hess, M., Koepke, P., and Schult, I.: Optical properties of aerosols and clouds: the software package OPAC, B. Am. Meteorol. Soc., 79, 831–844, doi:10.1175/1520-0477(1998)079<0831:OPOAAC>2.0.CO;2, 1998. 3378, 3379

Hong, G., Feng, Q., Yang, P., Kattawar, G. W., Minnis, P., and Hu, Y. X.: Optical properties of ice particles in young contrails, J. Quant. Spectrosc. Ra., 109, 2635–2647, doi:10.1016/j.jqsrt.2008.06.005, 2008. 3378

IPCC: Summary for policymakers, in: Climate Change 2013: The Physical Science Basis. Contribution of Working Group I to the Fourth Assessment Report of the Intergovernmental Panel on Climate Change, available at: http://www.ipcc.ch/report/ar5/wg1/ (last access: 14 May 2014), 2013. 3368

Jacobson, M. Z.: A physically-based treatment of elemental carbon optics: implications for global direct forcing of aerosols, Geophys. Res. Lett., 27, 217–220, doi:10.1029/1999GL010968, 2000. 3370, 3374, 3376, 3385, 3386

Jacobson, M. Z.: Strong radiative heating due to the mixing state of black carbon in atmospheric aerosols, Nature, 409, 695–697, doi:10.1038/35055518, 2001. 3370, 3383

Jöckel, P., Sander, R., Kerkweg, A., Tost, H., and Lelieveld, J.: Technical Note: The Modular Earth Submodel System (MESSy) – a new approach towards Earth System Modeling, Atmos. Chem. Phys., 5, 433–444, doi:10.5194/acp-5-433-2005, 2005. 3369

GMDD
7, 3367–3402, 2014

Jöckel, P., Tost, H., Pozzer, A., Brühl, C., Buchholz, J., Ganzeveld, L., Hoor, P., Kerkweg, A., Lawrence, M. G., Sander, R., Steil, B., Stiller, G., Tanarhte, M., Taraborrelli, D., van Aardenne, J., and Lelieveld, J.: The atmospheric chemistry general circulation model ECHAM5/MESSy1: consistent simulation of ozone from the surface to the mesosphere, Atmos. Chem. Phys., 6, 5067–5104, doi:10.5194/acp-6-5067-2006, 2006. 3369, 3375

Kim, D., Wang, C., Ekman, A. M. L., Barth, M. C., and Rasch, P. J.: Distribution and direct radiative forcing of carbonaceous and sulfate aerosols in an interactive size-resolving aerosol-climate model, J. Geophys. Res.-Atmos., 113, 16309, doi:10.1029/2007JD009756, 2008. 3370, 3383

Kirchstetter, T. W., Novakov, T., and Hobbs, P. V.: Evidence that the spectral dependence of light absorption by aerosols is affected by organic carbon, J. Geophys. Res.-Atmos., 109, D21208, doi:10.1029/2004JD004999, 2004. 3379

Lauer, A., Eyring, V., Hendricks, J., Jöckel, P., and Lohmann, U.: Global model simulations of the impact of ocean-going ships on aerosols, clouds, and the radiation budget, Atmos. Chem. Phys., 7, 5061–5079, doi:10.5194/acp-7-5061-2007, 2007. 3370, 3375

Mayer, B. and Kylling, A.: Technical note: The libRadtran software package for radiative transfer calculations - description and examples of use, Atmos. Chem. Phys., 5, 1855–1877, doi:10.5194/acp-5-1855-2005, 2005. 3375

Peña, O. and Pal, U.: Scattering of electromagnetic radiation by a multilayered sphere, Comput. Phys. Commun., 180, 2348–2354, doi:10.1016/j.cpc.2009.07.010, 2009. 3375

Pozzer, A., de Meij, A., Pringle, K. J., Tost, H., Doering, U. M., van Aardenne, J., and Lelieveld, J.: Distributions and regional budgets of aerosols and their precursors simulated with the EMAC chemistry-climate model, Atmos. Chem. Phys., 12, 961–987, doi:10.5194/acp-12-961-2012, 2012. 3370, 3375, 3379, 3383, 3384

Pringle, K. J., Tost, H., Message, S., Steil, B., Giannadaki, D., Nenes, A., Fountoukis, C., Stier, P., Vignati, E., and Lelieveld, J.: Description and evaluation of GMXe: a new aerosol submodel for global simulations (v1), Geosci. Model Dev., 3, 391–412, doi:10.5194/gmd-3-391-2010, 2010a. 3375

Pringle, K. J., Tost, H., Metzger, S., Steil, B., Giannadaki, D., Nenes, A., Fountoukis, C., Stier, P., Vignati, E., and Lelieveld, J.: Corrigendum to "Description and evaluation of GMXe: a new aerosol submodel for global simulations (v1)" published in Geosci. Model Dev., 3, 391–412, 2010, Geosci. Model Dev., 3, 413–413, doi:10.5194/gmd-3-413-2010, 2010b. 3375

GMDD
7, 3367–3402, 2014

Rothman, L. S., Jacquemart, D., Barbe, A., Chris Benner, D., Birk, M., Brown, L. R., Carleer, M. R., Chackerian, C., Chance, K., Coudert, L. H., Dana, V., Devi, V. M., Flaud, J.-M., Gamache, R. R., Goldman, A., Hartmann, J.-M., Jucks, K. W., Maki, A. G., Mandin, J.-Y., Massie, S. T., Orphal, J., Perrin, A., Rinsland, C. P., Smith, M. A. H., Tennyson, J., Tolchenov, R. N., Toth, R. A., Vander Auwera, J., Varanasi, P., and Wagner, G.: The HITRAN 2004 molecular spectroscopic database, J. Quant. Spectrosc. Ra., 96, 139, doi:10.1016/j.jqsrt.2004.10.008, 2005. 3379

Tanre, D., Geleyn, J.-F., and Slingo, J. M.: First results of the introduction of an advanced aerosol-radiation interaction in the ECMWF low resolution global model, in: Aerosols and their Climatic Effects, edited by: Gerber, H. and Deepak, A., A. Deepak Pub., 133–177, 1984. 3384

Toon, O. B. and Ackerman, T. P.: Algorithms for the calculation of scattering by stratified spheres, Appl. Optics, 20, 3657, doi:10.1364/AO.20.003657, 1981. 3374

Yang, W.: Improved recursive algorithm for light scattering by a multilayered sphere, Appl. Optics, 42, 1710–1720, doi:10.1364/AO.42.001710, 2003. 3374, 3375

GMDD
7, 3367–3402, 2014

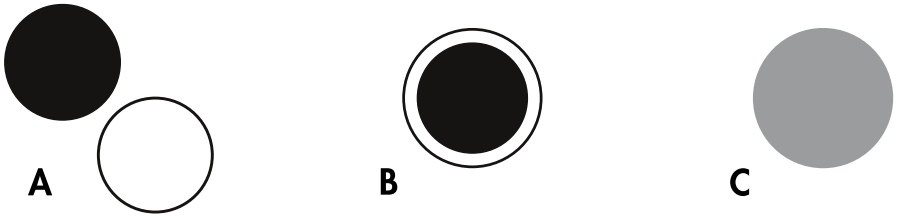

Figure 1. Schematic illustration of three mixing states. In externally mixed aerosols different types of particles coexist, each consisting of a single component **(A)** whereas in internally mixed aerosols the particles consist of a combination of components **(B, C)**. An internal mixture can be either inhomogeneous, e.g., having a core-shell structure **(B)** or homogeneous **(C)**. External mixtures **(A)** are least absorbing, as the increased cross section affected by absorbing components in an internal mixture **(B, C)** outweighs the decreased absorption efficiency.

GMDD
7, 3367–3402, 2014

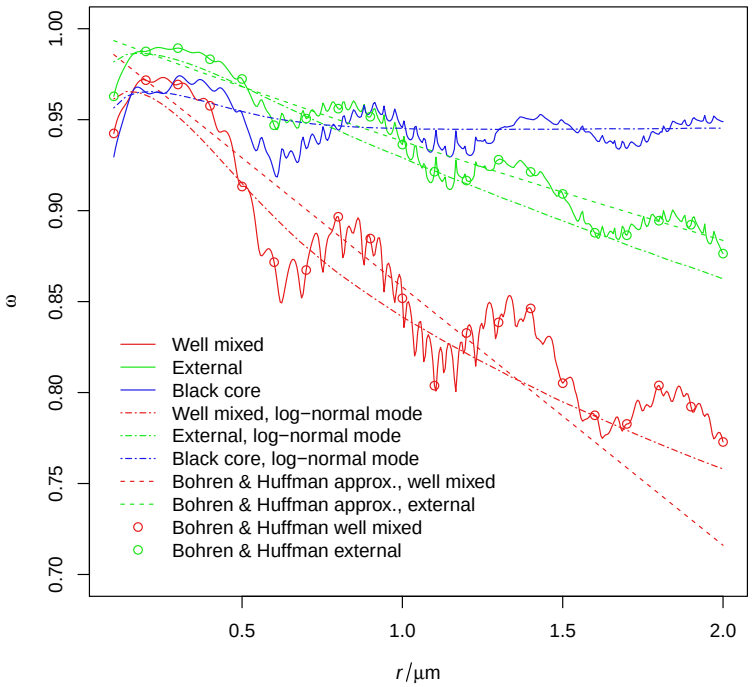

Figure 2. The single scattering albedo of a mixture of a "black" component ($m = 1.7 + i\ 0.7$, 1 % of the particle volume) and a "white" component ($m = 1.55 + i10^{-6}$, 99 % of the particle volume) assuming homogeneous internal mixing (red), external mixing (green) and core-shell particles (blue). The abscissa denotes the radius of the internally mixed particles and, in case of the external mixture, the white particles; the radius of the black particles is 0.05 µm. The results have been calculated using our new SCATTNLAY based AEROPT mixing algorithm for single size particles (solid) and log-normal size distributions ($\sigma_g = 1.59$, dash-dotted). In the latter case average mass radii are used. Also shown are analytic approximations (dashed) and numeric results (circles) from Bohren and Huffman (2007) for homogeneous internal and external mixtures. The wavelength is 0.55 µm.

GMDD
7, 3367–3402, 2014

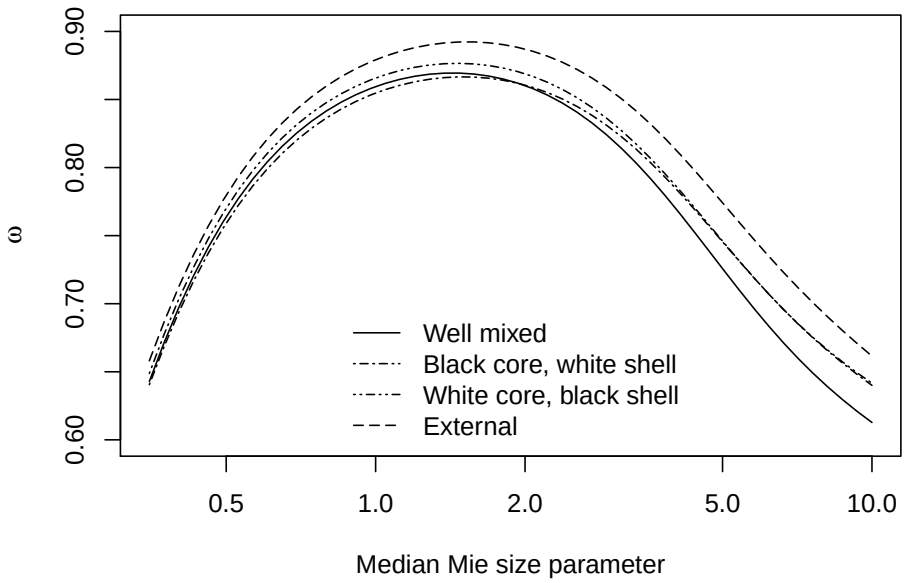

Figure 3. Single scattering albedo of a mixture of 2 % strongly absorbing matter with refractive index $m = 1.75+i0.43$ and 98 % less absorbing material with $m = 1.5+i0.02$. The particle radius is distributed according to a log-normal mode with geometric standard deviation $\sigma_g = 1.59$. Over the entire median Mie size parameter range, the internal mixtures with well mixed (volume average refractive index mixing rule) and core-shell particles are absorbing more efficiently than the external mixture. Depending on the median Mie size parameter x_{median}, absorption by core-shell particles with a black core is more ($x_{median} \lesssim 2$) or less ($x_{median} \gtrsim 2$) efficient than by well mixed particles. For all mixing states, left and right of the maximum, the single scattering albedo is very sensitive to the median Mie size parameter. Black coated spheres yield values between the result for internal and external mixing.

GMDD
7, 3367–3402, 2014

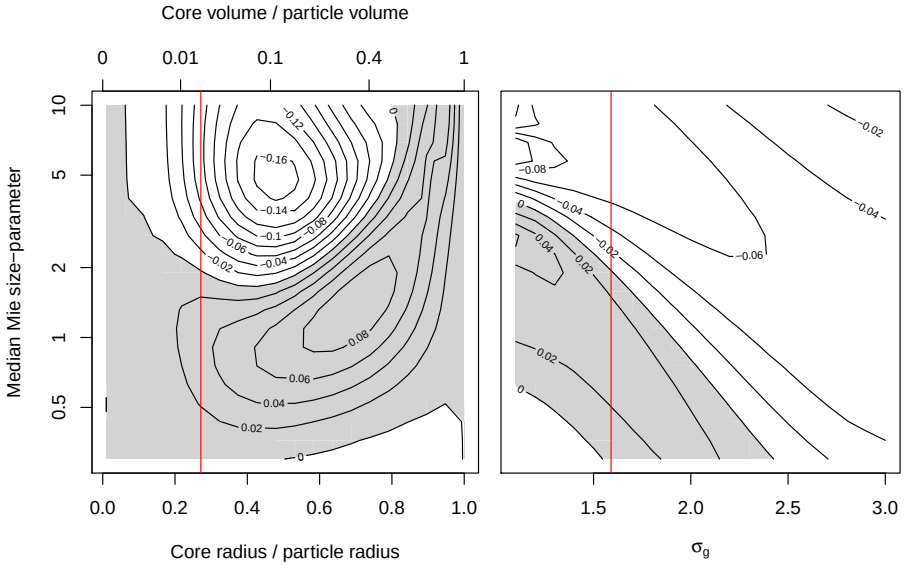

Figure 4. Relative difference of the absorption efficiency for well mixed and core-shell particles $(\omega_{\text{well mixed}} - \omega_{\text{core shell}})/(1 - \omega_{\text{well mixed}})$. The same components as in Fig. 3 are considered where the stronger absorbing component forms the core. In the left panel, the geometric standard deviation $\sigma_g = 1.59$ is used, whereas the mixing ratio is varied. In the right panel, the standard deviation σ_g is varied and the mixing ratio is the same as in Fig. 3. The solid red lines mark mixing ratio and variance, respectively, of the opposing panel. For well mixed particles, the volume average refractive index mixing rule is used.

GMDD
7, 3367–3402, 2014

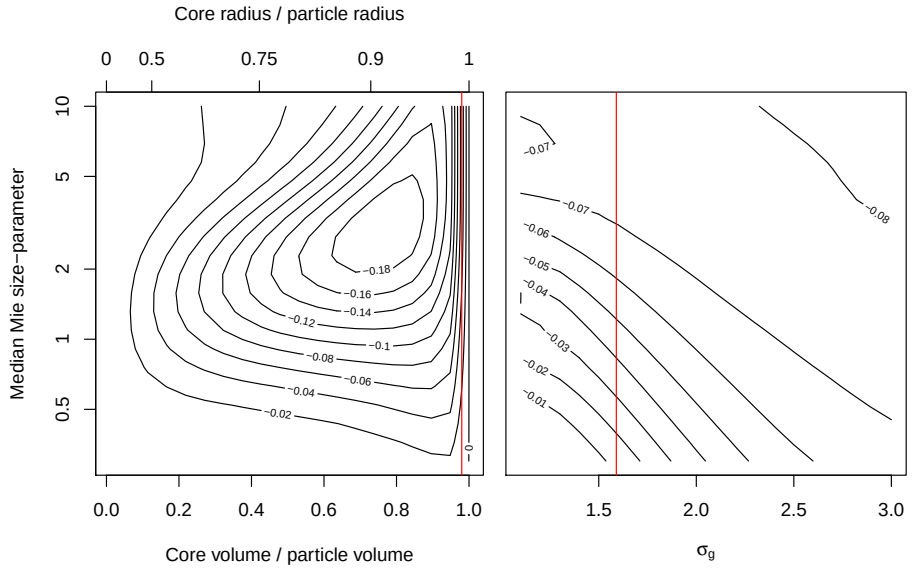

Figure 5. Same as Fig. 4 but with the stronger absorbing component coating the less absorbing component.

GMDD
7, 3367–3402, 2014

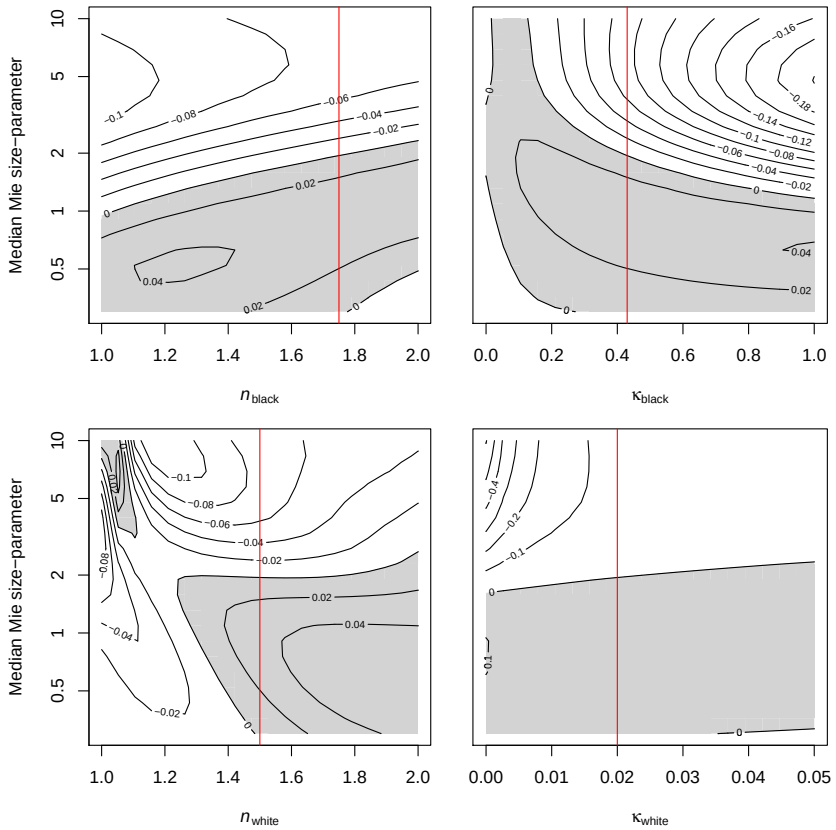

Figure 6. Relative difference of the absorption efficiency for well mixed and core-shell particles as in Fig. 4 for the geometric standard deviation $\sigma_g = 1.59$, 2 % black volume and varying refractive indices $m_{black} = n_{black} + i\kappa_{black}$ and $m_{white} = n_{white} + i\kappa_{white}$. The solid red lines mark the refractive indices used in the previous figures. For well mixed particles, the volume average refractive index mixing rule is used.

GMDD
7, 3367–3402, 2014

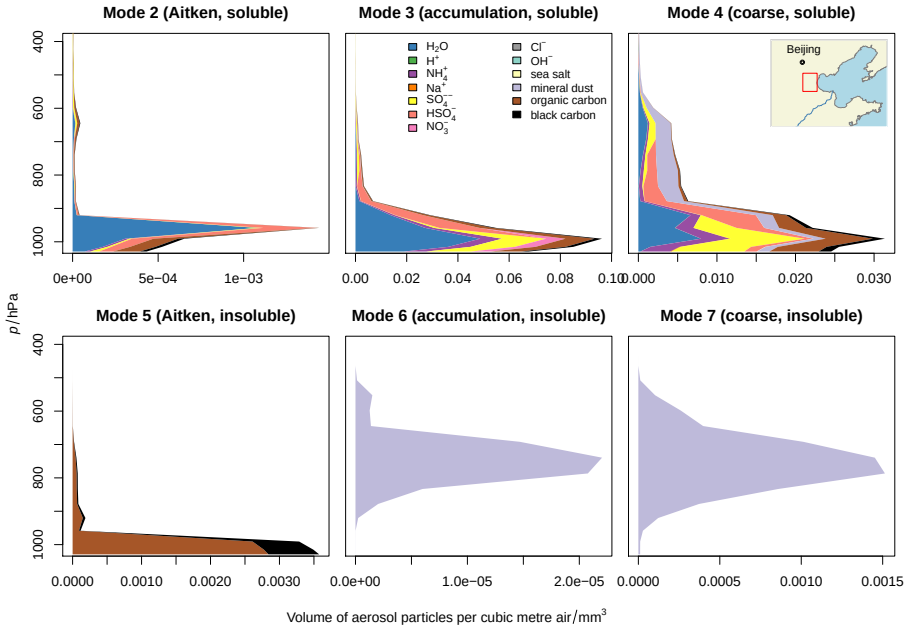

Figure 7. Vertical profiles of the aerosol concentrations in six modes over China which have been used as input for the column model when computing the optical properties in Fig. 8. The red rectangle in the inset of the top right figure depicts the area covered by the model column.

GMDD
7, 3367–3402, 2014

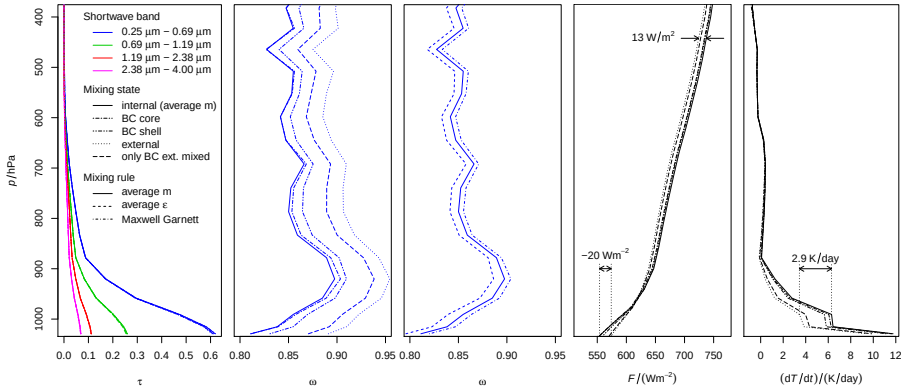

Figure 8. Column model results over China. From left to right: aerosol optical depth τ, single scattering albedo ω, single scattering albedo (alternative mixing rules), net shortwave flux F, temperature tendency $\mathrm{d}T/\mathrm{d}t$. The optical depth is shown for each shortwave band, whereas the single scattering albedo is shown only for the dominant band (0.25–0.69 µm). The flux takes all solar bands into account, the temperature tendency additionally the effects of terrestrial infrared radiation.

GMDD
7, 3367–3402, 2014

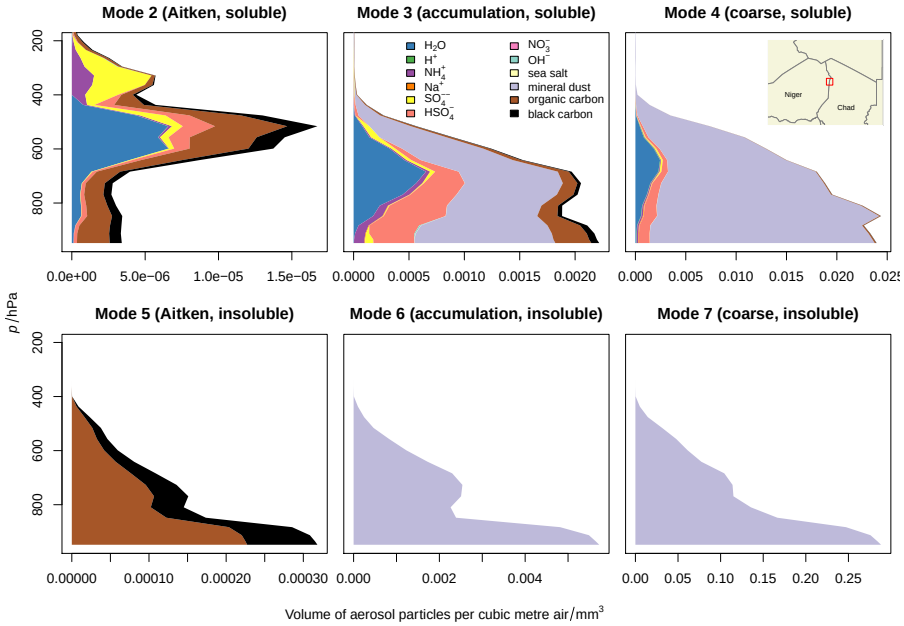

Figure 9. Vertical profiles of the aerosol concentrations in six modes over the Sahara which have been used as input for the column model when computing the optical properties in Fig. 10. The red rectangle in the inset of the top right figure depicts the area covered by the model column.

GMDD
7, 3367–3402, 2014

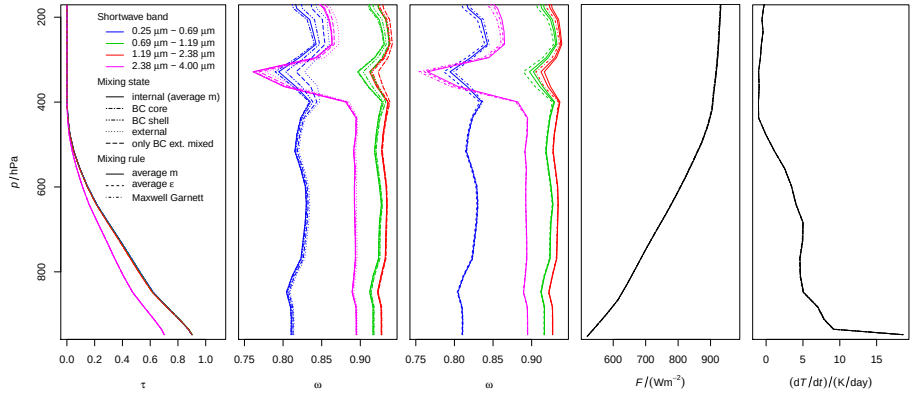

Figure 10. Column model results over the Sahara. From left to right: aerosol optical depth τ, single scattering albedo ω, single scattering albedo (alternative mixing rules), net shortwave flux F, temperature tendency $\mathrm{d}T/\mathrm{d}t$. The temperature tendency takes the terrestrial bands into account. In this example, the mixing state sensitivity is small so that the flux profiles and the temperature tendencies for the different mixing states coincide.

GMDD
7, 3367–3402, 2014

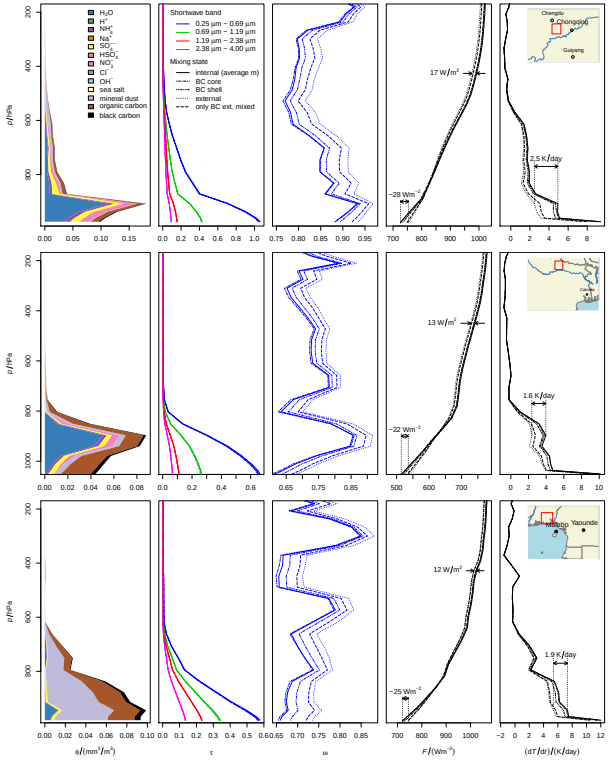

Figure 11. Column model results over (from top to bottom) the Sichuan Basin in China (29.72° N, 104.62° E, April), the Gangetic Plain in India (26.35° N, 84.37° E, November) and the eastern Niger Delta in Nigeria (5.05° N, 7.87° E, January). From left to right: aerosol concentrations, aerosol optical depth τ, single scattering albedo ω, net shortwave flux F, temperature tendency $\mathrm{d}T/\mathrm{d}t$. The optical depth is shown for each shortwave band, whereas the single scattering albedo is shown only for the dominant band (0.25–0.69 µm). The flux takes all solar bands into account, the temperature tendency additionally the effects of terrestrial infrared radiation.

GMDD
7, 3367–3402, 2014

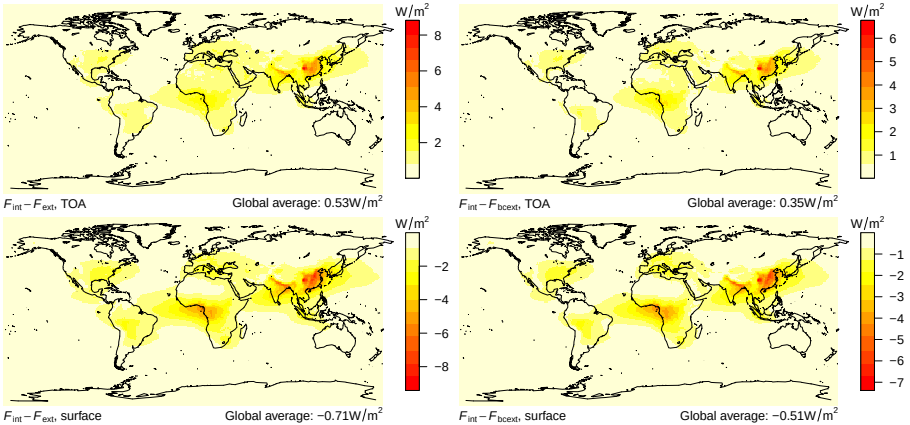

Figure 12. Difference in net shortwave flux between internal and external mixing $F_{int} - F_{ext}$ (top left) and between internal and intermediate mixing state $F_{int} - F_{bcext}$ (top right) at the top of the atmosphere, averaged over the year 2005. The bottom row shows the corresponding values at the surface.

GMDD
7, 3367–3402, 2014